Rapid production of ^{87}Rb Bose-Einstein condensates in a combined magnetic and optical potential

Y.-J. Lin, A. R. Perry, R. L. Compton, I. B. Spielman,* and J. V. Porto†
Joint Quantum Institute, National Institute of Standards and Technology and University of Maryland, Gaithersburg, Maryland 20899, USA
(Received 2 April 2009; published 29 June 2009)

We describe an apparatus for quickly and simply producing ^{87}Rb Bose-Einstein condensates. It is based on a magnetic quadrupole trap and a red-detuned optical dipole trap. We collect atoms in a magneto-optical trap (MOT) and then capture the atoms in a magnetic quadrupole trap and force rf evaporation. We then transfer the resulting cold dense cloud into a spatially mode-matched optical dipole trap by lowering the quadrupole field gradient to below gravity. This technique combines the efficient capture of atoms from a MOT into a magnetic trap with the rapid evaporation of optical dipole traps; the approach is insensitive to the peak quadrupole gradient and the precise trapping beam waist. Our system reliably produces a condensate with $N \approx 2 \times 10^6$ atoms every 16 s.

DOI: 10.1103/PhysRevA.79.063631 PACS number(s): 03.75.Hh, 67.85.Hj

I. INTRODUCTION

A range of techniques have been developed to produce quantum degenerate gases of varying degrees of complexity and difficulty. Almost all current methods rely on the same basic approach: laser cooling of atoms [1] followed by evaporative cooling in a conservative trap [2,3]. When designing there are many often competing considerations: reliability, speed, simplicity, large optical access, and reasonably large number. We describe here a simple approach that quickly produces a relatively large Bose-Einstein condensate (BEC) of ^{87}Rb atoms.

Magnetic quadrupole traps for neutral atoms [4] have several strengths. They have large trap volumes, which can be well matched to the size of laser-cooled atom clouds. The effectively linear potential provides tight confinement, allowing for efficient evaporative cooling, and the quadrupole field can be generated from a simple arrangement of two electromagnetic coils that allows for good optical access to the sample. The quadrupole trap's one major drawback is Majorana spin-flip losses and the resulting heating near the zero-field point at the center of the trap. This limits the forced evaporative cooling to relatively low phase-space densities [5]. Still, the first two dilute-gas BEC's were produced in traps derived from the simple quadrupole trap, taking advantage of its strengths by avoiding the Majorana losses in two different ways: by providing a time-orbiting bias field (time orbiting potential "TOP" trap) to shift the zero away from the atom cloud [2,6] or by using a repulsive optical potential (i.e., an optical plug) to push the atoms away from the zero [3]. The TOP trap is still widely used, and the optically plugged trap has successfully been revisited [7].

Far-detuned optical dipole traps have a different set of strengths. They can be spin-state independent, made in flexible geometries that provide good optical access, have tight confinement and efficient evaporation, and do not require magnetic coils. One drawback is that simultaneously deep and large-volume traps require prohibitively large laser power. One must carefully "mode match" the laser-cooled atoms to the optical dipole trap, and the all-optical approaches tend to produce relatively small BECs [8–10]. By loading into large-volume shallow traps and transferring into smaller volume traps [9], larger BECs can be made [11], but this requires superlative high-density laser cooling. It has been suggested that the BECs could be efficiently produced using a quadrupole trap as a reservoir to directly feed a red-detuned dipole trap [12]. We demonstrate here such a hybrid technique which combines the advantages of quadrupole and optical traps while avoiding their individual weaknesses. We can then load the BEC from the hybrid trap into an all-optical dipole trap without an additional blue-detuned optical plug.

The basic approach is to load laser-cooled atoms into a quadrupole trap and use forced rf evaporation [5] to increase the phase-space density until Majorana spin flips cause significant loss and heating. We then transfer atoms from the quadrupole trap to a single-beam optical dipole trap. This step can be fairly efficient, transferring a large fraction of the atoms from the quadrupole trap into the optical trap. To limit Majorana losses during and after the transfer, the center of the optical trap is offset by roughly a beam waist from the field zero of the magnetic trap. Further, offset quadrupole field provides harmonic confinement along the beam direction; this approach therefore yields three-dimensional (3D) confinement without a crossed dipole trap. Since the atom cloud is adiabatically cooled during the transfer, only a relatively small optical trap depth (~ 49 μK in our case) is required. The change in the trap shape during the adiabatic transfer, from linear quadrupole to harmonic, modifies the density of states in such a way as to increase the phase-space density at constant entropy, leading to fairly high initial phase-space density in the dipole trap. Forced evaporative cooling by lowering the optical trap power [8] then leads to quantum degeneracy. This scheme is simple and flexible and allows for significant optical access. We reliably produce ^{87}Rb BECs with $N = 2 \times 10^6$ atoms in a time $t \approx 16$ s.

*ian.spielman@nist.gov
†trey@nist.gov

 ©2009 The American Physical Society

II. THEORY

In order to discuss this approach, we first provide a brief overview of trapped gas thermodynamics and cooling for our trap geometry. (More detailed discussions can be found in Refs. [13,14] and further references therein.) The thermodynamic properties of the gas are determined by the partition function $\zeta = V_0/\Lambda^3$, where $\Lambda = (2\pi\hbar^2/mk_BT)^{1/2}$ is the thermal de Broglie wavelength and

$$V_0 = \int \exp[-U(\mathbf{r})/k_BT]d^3r \tag{1}$$

is an effective trap volume, where $U(\mathbf{r})$ is the trapping potential with the energy minimum $U(\mathbf{r}_{\min})=0$ at position $\mathbf{r}_{\min}$, and T is the temperature. Corrections to V_0 due to the finite trap depth $\epsilon_t = \eta k_BT$ during evaporation can be treated using a truncated Boltzmann distribution [13], where η is the truncation parameter. The large-η limit [Eq. (1)] is reasonable for most purposes when $\eta \gtrsim 8$, and below this range it provides a qualitative description. From ζ and V_0, one can calculate, for example, the free energy $A = -Nk_BT \ln \zeta$, the entropy $S = -\partial A/\partial T$, the peak phase-space density $D = N/\zeta$, and the density distribution

$$n(\mathbf{r}) = n_0 \exp[-U(\mathbf{r})/k_BT] = \frac{N}{V_0}\exp[-U(\mathbf{r})/k_BT]. \tag{2}$$

Dynamic rates relevant for evaporation, such as n-body loss, collision rates, evaporation rates, etc., can be calculated from similar integrals [13].

The effective potential for atoms in the combined quadrupole plus dipole trap, including gravity, is

$$U(\mathbf{r}) = \mu B' \sqrt{\frac{x^2}{4} + \frac{y^2}{4} + z^2} - U_0 \times \exp\{-2[x^2 + (z-z_0)^2]/w_0^2\} + mgz + E_0, \tag{3}$$

where B' is the quadrupole field gradient along $\hat{z}$, U_0, w_0, and z_0 are the dipole beam trap depth, waist, and offset from the zero-field point at $x,y,z=0$. E_0 is the energy difference between the zero-field point absent the dipole trap and the total trap minimum, giving the trap minimum $U(\mathbf{r}_{\min})=0$, μ and m are the magnetic moment and mass of the atom, respectively, and g is the acceleration due to gravity. Here the dipole beam is aligned along $\hat{y}$ and is displaced vertically (along $\hat{z}$) below the magnetic field zero. (We have ignored the focusing of the beam along $\hat{y}$ since for our waist $w_0 = 65$ μm the Rayleigh length $\pi w_0^2/\lambda \approx 9$ mm is large.) The effective volume as a function of temperature can be calculated from Eq. (1).

At high temperature, by approximating $U(\mathbf{r})$ as

$$U(\mathbf{r}) \simeq \mu B' \sqrt{\frac{x^2}{4} + \frac{y^2}{4} + z^2} + E_0 + mgz, \tag{4}$$

we have

$$V_0(T) \simeq \frac{32\pi e^{-E_0/k_BT}}{[1-(mg/\mu B')^2]^2}\left(\frac{k_BT}{\mu B'}\right)^3, \quad \text{for } T \gg U_0/k_B, \tag{5}$$

where $E_0 \simeq U_0$ for a typical dipole beam offset $z_0 \simeq -w_0$. This approximation is only valid for field gradients that compensate gravity, $\mu B' > mg$. The thermodynamic effect of gravity can be viewed as rescaling the field gradient to $\mu B'_{eff} = \mu B'[1-(mg/\mu B')^2]^{2/3}$, which vanishes at $\mu B' = mg$. In the absence of the dipole trap and ignoring gravity, the effective volume reduces to the simple quadrupole form $V_0(T) = 32\pi(k_BT/\mu B')^3$, but for most parameters we encounter, both corrections are important.

At low temperature the dipole potential can be approximated as a harmonic trap

$$U(\mathbf{r}) \simeq \frac{1}{2}[U_x''x^2 + U_y''y^2 + U_z''(z-z_{\min})^2], \tag{6}$$

where U_i'' are the curvatures at the bottom of the total trap, and the trap minimum is at position $z_{\min}$. This gives

$$V_0(T) \simeq \frac{(2\pi k_BT)^{3/2}}{\sqrt{U_x''U_y''U_z''}}, \quad \text{for } T \ll U_0/k_B. \tag{7}$$

The curvatures along $\hat{x}$ and $\hat{z}$ are dominated by the dipole trap, $\omega_{x,z} \simeq 2\sqrt{U_0/mw_0^2}$, and the curvature along $\hat{y}$ is dominated by the magnetic trap, $\omega_y = (1/2)\sqrt{\mu B'/mz_{\min}}$. We perform a numerical integration for the volume V_0 [from Eq. (1)] and entropy S, as shown in Fig. 1. Both the high- and low-temperature approximations for the V_0 and S are quite good over a range of temperatures. The high-temperature approximation is accurate well below U_0/k_B.

The success of our hybrid approach depends critically on managing two processes: limiting Majorana loss in the quadrupole trap and effective adiabatic (approximately constant entropy) transfer from the quadrupole trap to the harmonic dipole trap. Majorana loss is particularly detrimental, as it causes both loss and heating. Such loss can be difficult to describe accurately, but a simple argument [6] leads to the estimate that the Majorana loss rate Γ_m scales as $\Gamma_m \propto \hbar/ml^2$, where l is the radial half-width half maximum cloud size in the quadrupole trap. Using the proportionality constant measured in [6], we can estimate

$$\Gamma_m = 3.6\frac{\hbar}{ml^2} = 1.85\frac{\hbar}{m}\left(\frac{\mu B'}{k_BT}\right)^2, \tag{8}$$

where we have ignored gravity. This estimate is independent of the elastic collision rate in the trap since it assumes thermal equilibrium, an invalid assumption at low densities or large loss rates. Nonetheless, it suggests that for field gradients of ~ 1.40 T/m, the lifetime should be on the order of 1 s at 20 μK. Near this temperature fast evaporation (high elastic collision rate) is advantageous. This loss rate can be mediated somewhat by adiabatically expanding the trap since the temperature scales more weakly than the field gradient at constant entropy, $T \propto (B')^{2/3}$, and weakening the trap will decrease the loss rate at the expense of a lower collisional rate.

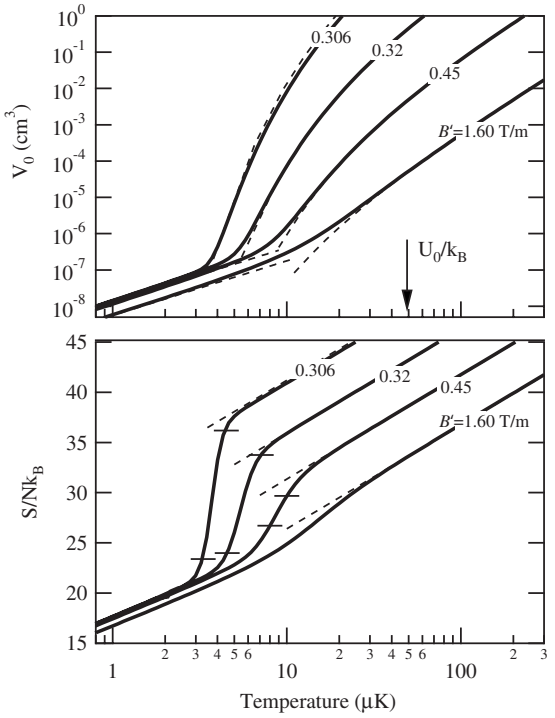

FIG. 1. Top: V_0 as a function of temperature for several different field gradients. Thick lines: numerical calculation for field gradients $B'=1.60$, 0.45, 0.32, and 0.306 T/m. (For ^{87}Rb magnetically trapped in $|F,m_F\rangle=|1,-1\rangle$, $mg=\mu\times 0.304\ 92$ T/m.) Dashed lines: analytical approximations [Eqs. (5) and (7)]. The dipole trap depth for all plots (indicated by the arrow) is $U_0/k_B=49$ μK, and the beam waist is 65 μm along $\hat{x}$ and 78 μm along $\hat{z}$ (which accounts for the difference in measured trap frequencies along $\hat{x}$ and $\hat{z}$). Bottom: the entropy per particle, $S(T)/Nk_B$, for the same field gradients in the dipole-plus-quadrupole trap (solid lines) and for analytic approximation based on Eq. (5) (dashed lines). The short horizontal marks crossing the curves indicate the regions where the atoms are transferred into the dipole trap: the upper set marks where 10% of the atoms are in the dipole trap, and the lower set marks where 90% of the atoms are in the dipole trap.

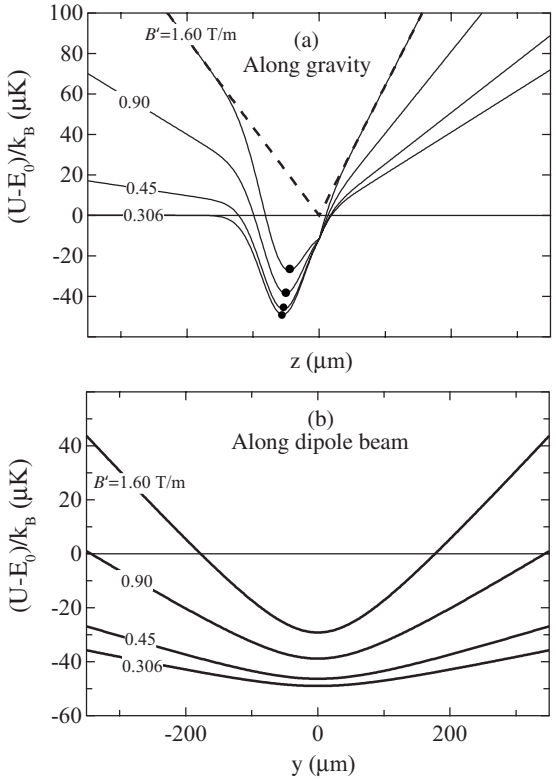

FIG. 2. Cross sections of trapping potential with the offset E_0 subtracted, $U(\mathbf{r})-E_0$, at several points during an adiabatic expansion ($B'=1.60$, 0.90, 0.45, and 0.306 T/m): (a) along $\hat{z}$ (gravity is along $-\hat{z}$) at $x,y=0$, the potential minima $z=z_{\min}$ are indicated by filled circles, and (b) along $\hat{y}$ (the dipole beam direction) at $x=0$, each taken at $z=z_{\min}$. The dashed line is the potential at 1.60 T/m without the dipole trap. The dipole trap parameters are the same as for Fig. 1.

The adiabatic transfer is more subtle than a mere expansion of the trap volume since in addition to expanding the trap the shape of the trap is modified. This leads to changes in phase-space density even at constant entropy [15], an effect used to obtain a BEC of cesium from a very cold but dilute gas [9]. In our case, the effect is quite strong as the transfer process both decreases the temperature and increases phase-space density.

The trap potential during an example expansion sequence is shown in Fig. 2. The change in the trap from linear to quadratic dramatically changes the dependence of the entropy on temperature, from $S\propto \ln T^{9/2}$ at high T and B' to $S\propto \ln T^3$ at low T and B' (see Fig. 1). The crossover temperature, T_x, between these two regimes occurs roughly when the high- and low-temperature approximations for $V_0(T)$ [Eqs. (5) and (7)] are equal. The steep nature of $S(T)$ near T_x for $\mu B'\simeq mg$ indicates that adiabatic expansion from a wide range of initial temperatures leads to a roughly constant final $T\simeq T_x$, which is about $0.1U_0/k_B$. The steep part of $S(T)$ near T_x also corresponds to the region over which the atoms are transferred into the dipole trap. Above the crossover region, a negligible fraction of atoms are in the dipole trap, but below this region, nearly all the atoms are in the dipole trap.

The adiabatic expansion and transfer are similar to forced evaporation except that here the "evaporated" atoms during the expansion are contained in the low-density tails of the weakly confining quadrupole trap, which will leave the trap after the quadrupole field gradient B' drops below gravity mg/μ. Many considerations are similar to evaporation, such as the final temperature being set by the dipole trap "depth" for temperatures $T_x\simeq 0.1U_0/k_B$. The ratio $\simeq 0.1$ is insensitive to U_0 and w_0 and is approximately a constant for $10<U_0<45$ μK with $w_0=65$ μm and for $65<w_0<190$ μm with $U_0=45$ μK. As with evaporation, there is, in principle, no upper bound on the efficiency of the process [14] so that nearly all the atoms could be cooled in the dipole trap from any initial temperature. This would take nearly infinite time, however, and in practice the adiabaticity of the actual process depends on the elastic collision rates throughout the trap. For $B'>mg/\mu$, once B' is lowered such that the expansion is nonadiabatic to the atoms in the low-density tails, the atoms are less efficiently transferred from the magnetic trap into the dipole trap. The atoms in the low-density tails are not detected in the absorption imaging and thus accounted as

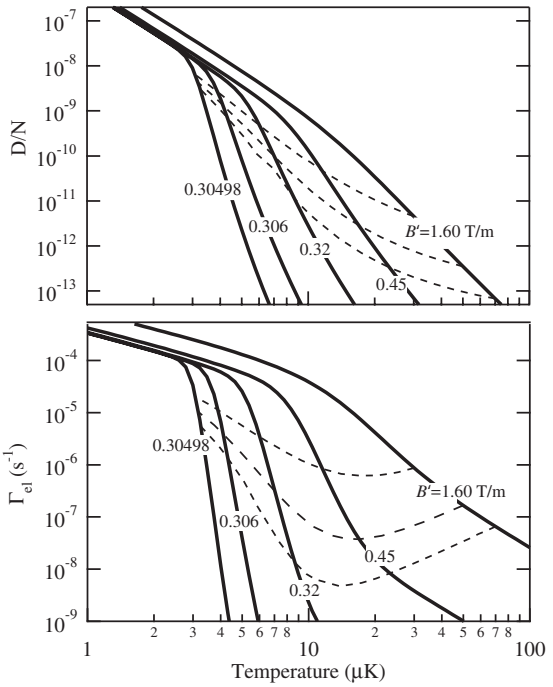

FIG. 3. Top: the phase-space density per particle $D(T)/N$ in the dipole-plus-quadrupole trap for the same field gradients as in Fig. 1, assuming no loss and thermal equilibrium (solid lines). Example of adiabatic trajectories for $D(T)/N$ calculated at constant entropy starting at $B'=1.6$ T/m are shown for different starting temperatures 30, 50, and 70 μK (dashed lines). Bottom: the average elastic collision rate Γ_{el}/N for the same field gradients (solid lines). The collision rate is shown for the same constant entropy trajectories as above (dashed lines).

a loss. Therefore, this inefficient evaporative loss will be more pronounced for a trap at lower densities with lower elastic collision rates.

Figure 3 shows the phase-space density per particle, D/N, as a function of temperature for a range of B'. To illustrate the expansion, several trajectories at constant entropy are shown for a few different initial temperatures. These plots show that if thermal equilibrium could be maintained and absent any loss mechanism, extremely large increases in phase-space density are possible. In practice, the collision rate in the low-density tails of the atom cloud eventually drops too low to maintain equilibrium. The actual efficiency of the process, and the optimal trajectory, will depend on this decoupling, as well as the Majorana and one-body loss due to collision with atoms in the background gas.

III. EXPERIMENT

The cooling process begins with a thermal beam of rubidium atoms cooled and decelerated by a zero crossing Zeeman slower. The slowed atoms are loaded into a six beam MOT and then transferred to the magnetic quadrupole trap where they are cooled by forced rf evaporation. In the final stage of cooling the atoms are transferred into the hybrid optical dipole plus magnetic trap where they reach degeneracy.

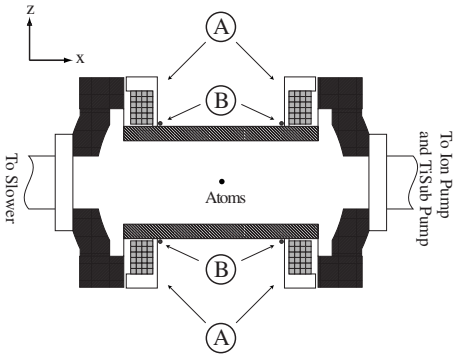

FIG. 4. Cut-away diagram of the main chamber. The main chamber is equipped with recessed windows in which we have mounted (a) 24 turn water-cooled coils and (b) single turn rf evaporation loops.

A. Vacuum system

Our apparatus consists of two ultrahigh vacuum (UHV) zones: a rubidium oven and the main experimental chamber. Each chamber is pumped with a single 55 L s^{-1} ion pump. In addition, the experimental chamber is pumped with a titanium sublimation (TiSub) pump attached to a bellows mounted orthogonally to the slower axis. When operated, the TiSub filament can be translated and positioned directly in line with Zeeman slower, allowing it to coat part of the inside of the main vacuum chamber near the slower entrance while avoiding the optical windows of the chamber. After evaporation it is retracted from the slower axis.

The oven is separated from the main experimental chamber by an in-vacuum shutter, a differential pumping tube (1.1 cm inner diameter, 7 cm long), a pneumatic gate valve (normally open), and the Zeeman slower (a 0.9 m long stainless tube with a 3.5 cm inner diameter). Together these tubes give a calculated conductance of 1.3 L s^{-1} [16]. The differential pumping between the chamber and the oven allows the chamber pressure to be significantly below the oven pressure. The oven has a nominal pressure of 5×10^{-10} mbar measured using the ion pump current. The ion pump current in the experimental chamber is zero to the accuracy of the pump controller.

The main chamber consists of a single stainless steel assembly with two 14-cm-diameter-recessed windows in the top and bottom (Fig. 4). The windows are recessed as much as possible without blocking the line of sight from the remaining 16 miniconflat ($d=3.8$ cm) and 6 larger conflat ($d=7$ cm) viewports.

B. Oven

The rubidium atomic beam originates from a heated rubidium reservoir (Fig. 5) and is collimated before entering the Zeeman slower. Efficient collimation is desirable since it lengthens the time between rubidium reloads and extends the lifetime of the ion pump.

The rubidium reservoir is contained within a 7.5-cm-long stainless steel (SS) bellows and was initially loaded with a 5 g rubidium glass ampule. The ampule is broken under vacuum after baking. During operation the reservoir is held

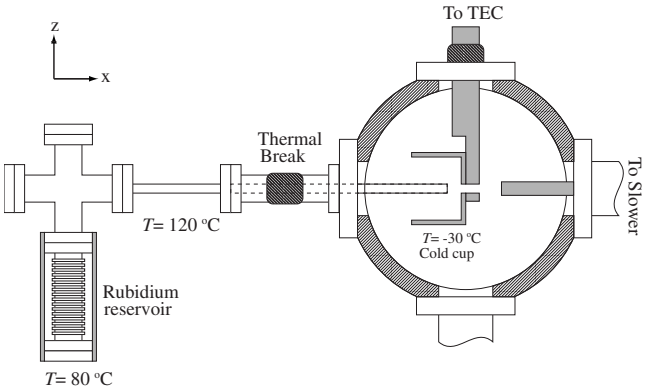

FIG. 5. Schematic diagram of rubidium oven. The left portion of the figure shows the heated rubidium oven indicating the regions of different temperature. The right part of the figure is a cut away of the main oven chamber showing the end of the collimation tube and the in-vacuum cold cup.

at 80 °C, setting the rubidium vapor pressure $\approx 6 \times 10^{-5}$ mbar and the mean free path (MFP) to be $\lesssim 1$ m (molecular flow regime everywhere).

The reservoir is connected to a four-way miniconflat style cross and then to the collimating tube. The SS collimation tube has a 6 mm diameter and is about 22.5 cm in length. The four-way cross and the first 7.5 cm of the collimation tube are maintained at 120 °C, providing a thermal gradient between the reservoir and the collimation tube. The remaining 15 cm experiences a thermal gradient due to the balance of thermal conduction and black-body radiation; we estimate the temperature of the free end of the tube to be 70 °C (all points in the tube are above rubidium's 39 °C melting point). The oven chamber is thermally isolated from the

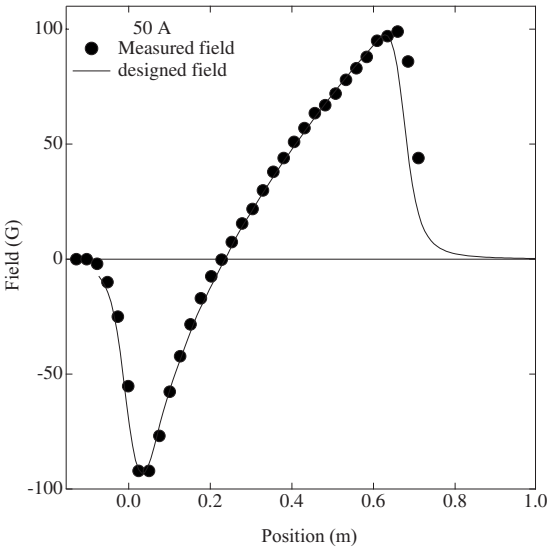

FIG. 6. Comparison of the calculated (continuous curve) and measured field profile (points) for our Zeeman slower. The measurement was performed with 50 A in both the forward and reverse portions of the slower which would result in slowing at 50% of the peak acceleration. (We found the optimum operating condition to be 72 A in the positive field portion and 42 A in the negative field region.)

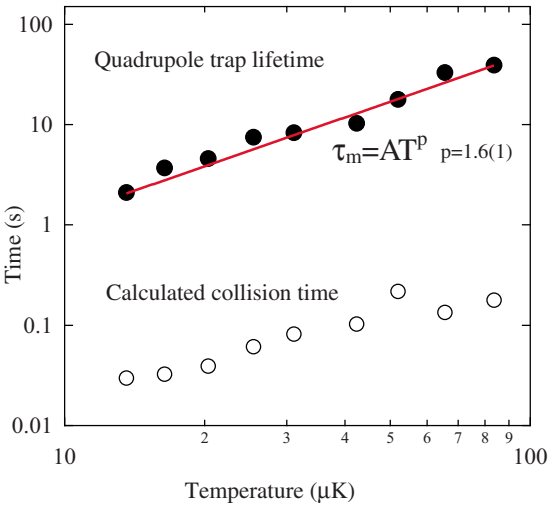

FIG. 7. (Color online) Lifetime τ_m and collision times Γ_{el}^{-1} in the compressed quadrupole trap at the field gradient $B' = 1.55$ T m^{-1}. Solid circles: measured lifetime in the quadrupole trap showing the Majorana losses. Empty circles: calculated collision time from measured number and trap parameters.

120 °C oven by a glass thermal break. This oven is not a recirculating design [17–19], but we expect that the elevated temperature of the collimation tube with respect to the reservoir keeps the tube free of rubidium.

We estimate that the collimation by the tube provides about a 25× improvement in flux directed into our MOT compared to a simple aperture with the same total flux [20]. We estimate that 1% of all atoms departing the oven fall within the ≈ 1 cm radius of the MOT beams (neglecting the transverse heating and expansion of the beam from the Zeeman slowing process).

The outgoing atomic beam first passes through a 6 mm aperture in a copper cold cup; after a further 2 cm the beam proceeds through an in-vacuum shutter (not pictured),

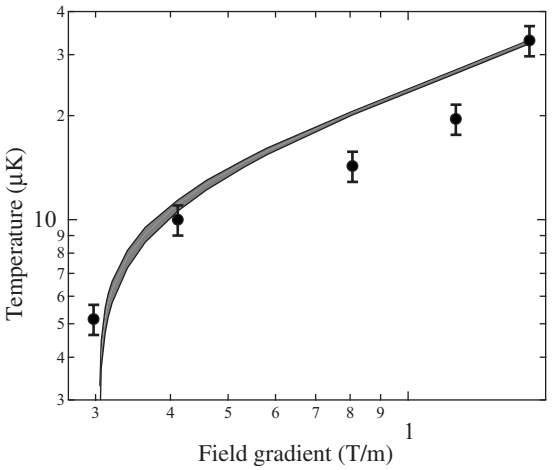

FIG. 8. Temperature T versus quadrupole field gradient B' during the transfer into the dipole trap. Circles indicate the measurement, where the data point at the lowest T corresponds to the end of the transfer at $\mu B' < mg$, and thus free evaporation. For comparison, the shaded region denotes calculation for a constant entropy per atom, with the uncertainty from dipole trap parameters.

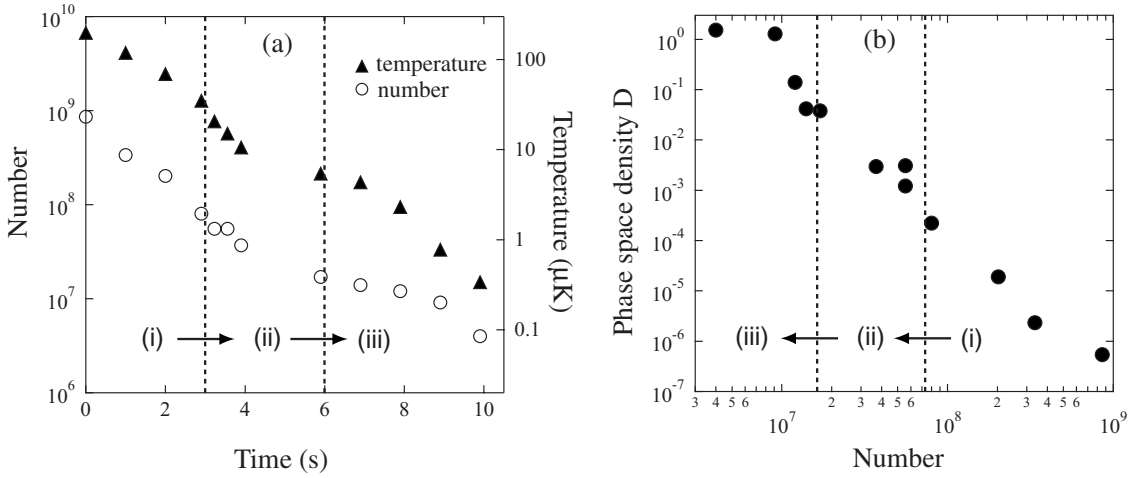

FIG. 9. Rapid production of a BEC of $N=2\times10^6$ atoms from step (i) to (iii). (i) rf evaporation in the compressed quadrupole trap, (ii) loading into the dipole trap, and (iii) evaporation in the dipole trap. (a) Atom number N (open circles) and temperature T (solid triangles) versus the trapping time. (b) Peak phase-space density D versus N.

through a differential pumping tube, and then enters the Zeeman slower. The cold cup is chilled to ≈ -30 °C by a commercial thermoelectric (TEC) based CPU cooler and the thermal link into the vacuum chamber is a high current vacuum feed thru. We find that the cold cup capturing excess rubidium is essential to the long-term operation of our ion pumps, which can fail due to excess leakage current as they pump rubidium (similar alkali poisoning has been observed elsewhere [21]). Even for the collimated beam, nearly half of the outgoing rubidium is incident on the cold cup.

To further inoculate our oven ion pump from rubidium poisoning, we permanently maintain the pump at 70 °C to drive off rubidium. As of this writing, the oven with its initial 5 g rubidium sample has been under vacuum and operating essentially daily since 2006, with an operating pressure of 5×10^{-10} mbar.

C. Zeeman slower

We slow and cool the collimated atomic beam using a Zeeman slower [22]. Operating at maximum efficiency and with an optimal field profile, our 69 cm long slower would stop rubidium atoms with a peak velocity $v_{\max}=390$ m s^{-1} losing about 67×10^3 photon recoil momenta ($\lambda=780$ nm). Our realized slower operates at nearly 70% of the maximum deceleration.

The slower field profile is a zero crossing design [23] and is generated from two single-layer helically wound coils which provide the positive and negative sections of the field profile. We modeled the field profile for the full variable-pitch coils and found an optimized winding pattern with 84 total turns (54 and 30 turns for the positive and negative field regions, respectively). Ideally, the optimized designed profile would slow atoms up to 84% of the maximum acceleration. The coils were wound from electrically insulated 1/8 in. (3 mm) diameter copper refrigerator tubing onto a $d=7.6$ cm aluminum form enclosing the conflat vacuum tube. In operation, cooling water forced through the copper tubes removes the heat dissipated by the 72 and 42 A flowing through the positive and negative field portions of the slower, respectively.

The calculated and measured field profiles are shown in Fig. 6. (An additional compensation coil, located beyond the end of the slower, zeros the field in the region of the MOT is not shown.) While a multilayer design could more optimally match the design field profile [24], we opted for the simplicity afforded with a single layer coil.

The Zeeman shifted atoms are slowed by a 30 mW laser beam counterpropagating with respect to the atomic beam (the slower laser has σ^+ polarization referenced to the positive field region of the slower). This laser is detuned 162 MHz below the $|5S_{1/2},\ F=2,m_F=2\rangle$ to $|5P_{3/2},\ F=3,m_F=3\rangle$ ^{87}Rb cycling transition. It enters the Zeeman slower with a 1 cm $1/e^2$ radius and reaches a focus in the oven collimation tube. A 15 mW repump laser beam, copropagating with the slower laser, prepares and maintains the atoms in the cycling transition. This σ^- repump beam is detuned 165 MHz below the $|5S_{1/2},F=1\rangle$ to $|5P_{3/2},F=2\rangle$ transition and is resonant with the slowed atoms in the low-field portions of the slower. We find that the performance of the slower is fairly insensitive to ≈ 50 MHz changes in the repump detuning.

The rubidium beam entering the slower is at $T\approx400$ K set by the 120 °C portions of the oven. Assuming a Maxwell-Boltzmann distribution the most probable velocity is $v=340$ m s^{-1}. Operating at about 70% of the maximum acceleration for rubidium, the peak capture velocity is 280 m s^{-1}, indicating we can slow 25% of ^{87}Rb atoms in the full distribution.

D. Magneto-optical trap

We capture our Zeeman slowed beam of atoms in a six beam MOT at the center of the main chamber, 15 cm from the end of the slower. The required quadrupole magnetic field is generated from the same coils used for magnetic trapping. For the MOT we run 25 A in the quadrupole coils, giving a field gradient of $\simeq 0.12$ T m^{-1} along $\hat{z}$.

Each of the six MOT beam has about 20 mW of power and are detuned by −21.5 MHz (3.5 linewidths) from the cycling transition. The MOT repumper has a total of 16 mW of power and is detuned by −5 MHz from the $|F=1\rangle$ to $|F=2\rangle$ transition. The MOT cooling and repumping light is combined in fiber, and each of the six beams are separately collimated. The six collimated MOT beams are directed into the vacuum chamber by reflecting them from moveable flipper mirrors, which can be moved out of the optical path after the atoms have been transferred to the magnetic trap and the MOT light is no longer needed. This provides optical access for beams needed in the experiment once the BEC has been made.

The MOT loads to $N=9\times10^8$ atoms in 3 s and saturates to about 2.7×10^9 atoms in 20 s. We infer the atom number by collecting light scattered from the MOT. (When the cloud is optically thick this can underestimate the total number of atoms.) After 3 s of MOT loading, we perform the polarization gradient cooling by turning off the magnetic trap, decreasing the intensity of the repump power to 100 μW, and linearly increasing the detuning of the MOT beams to 114 MHz (19 linewidths) over the course of 19 ms. At the end of the ramp the cloud has a temperature of 29(6) μK [25]. We then completely extinguish the repump light, depumping the atoms into the $F=1$ manifold.

E. Magnetic trap

Once the atoms are laser cooled, we transfer them to the hybrid of magnetic quadrupole and optical dipole trap. The quadrupole trap is constructed from a pair of 24 turn coils placed within recessed windows above and below the main vacuum chamber (Fig. 4). The coils are wound from the Kapton insulated 3/16 in. (0.48 cm) hollow square copper tube. We flow water through the coils in parallel with a pressure differential of about 14 bar (200 psi) to remove the ≈4.8 kW dissipated in the coils at a full current of 320 A. The coils can be effectively modeled as two 24 turn loops separated by 12 cm and each with a 5.8 cm radius. (This is not the ideal anti-Helmholtz configuration that could be realized by further recessing our top and bottom windows. Such recessing would have obscured optical access.) We measured a gradient of 4.8 mT m^{-1} A^{-1} in the stiff direction (vertical).

We capture our laser-cooled atoms by abruptly turning on the magnetic trap. For our MOT parameters, the optimal field gradient for best BEC production was 0.48 T m^{-1} along $\hat{z}$. Compressing to 1.6 T m^{-1} in 0.1 s increases the collisional rate and heats the atoms to 190(35) μK. Simultaneously with adiabatic compression, we turn on a dipole beam along $\hat{y}$ to increase the density and therefore the evaporation speed. The calculated peak collision rate and phase-space density are 15 s^{-1} and 5×10^{-7}. We then turn on the rf and apply a linear sweep of the frequency from 20 MHz down to 3.75 MHz in 2.9 s. During this rf-forced evaporation, the temperature and number decrease to 30(5) μK and $N=8\times10^7$ and the calculated density increases to 4.5×10^{12} cm^{-3}.

To characterize the loss from the Majorana spin flips, we measure the quadrupole trap lifetime τ_m versus the temperature T at $B'=1.55$ T m^{-1} without the dipole trap (Fig. 7). During the lifetime measurement at each T, we apply a rf knife to maintain a constant T given the heating from the Majorana spin flips. At our densities the calculated collision time is approximately 200 times shorter than τ_m, which ensures thermal equilibrium. τ_m is found to scale as $\tau_m=AT^p$ with the best fit of $p=1.6(1)$. A fit with fixed $p=2.0$ yields $A=5.8\times10^{-3}$ s μK^{-2}, approximately a factor of 2 of that given by Eq. (8), which was calibrated at a ≈50% larger field gradient, $B'=2.4$ T m^{-1}.

F. Transfer to the dipole trap

Next, we adiabatically ramp down the quadrupole field gradient B' from 1.6 to 0.30 T m^{-1} in 3 s, leaving the rf power on and ramping down the frequency to 2 MHz within the first 1 s, after which it remains constant. We turn off the rf at the end of the magnetic decompression when B' is smaller than the gravity, $mg/\mu=0.305$ T m^{-1}, and therefore loading the atoms into the dipole trap. The 3.5 W, $\lambda=1550$ nm dipole beam has a waist $w_0=65$ μm. We offset the center of dipole beam by $z_0\sim-w_0$ from the zero of magnetic field in order to decrease the Majorana loss, where the reduction factor scales as the density ratio $n(0)/n(\mathbf{r}_{\min})=\exp(-E'/k_BT)$, where $n(0)$ and $n(\mathbf{r}_{\min})$ are the densities at zero-field point and at the trap center $\mathbf{r}_{\min}$, respectively, and E' is the energy difference between $\mathbf{r}=0$ and $\mathbf{r}_{\min}$. We transfer the atoms into the dipole trap with a depth $U=49(6)$ μK and $E'=36(5)$ μK. The trap frequencies are 270 and 320(30) Hz along $\hat{x}$ and $\hat{z}$, respectively, and 30 Hz along $\hat{y}$ which is provided by the magnetic confinement at a field of 20 μT along $\hat{z}$ at the trap bottom.

We make the offset $z_0<0$ by moving the zero of magnetic field above the dipole beam by $-z_0$. We determine the dipole beam position by imaging the atoms (along the beam direction) in a tight dipole trap with the quadrupole field gradient $B'\sim mg/\mu$, where the sag of position along $\hat{z}$ is negligible. The position stability of our dipole beam derived from an acoustic-optical modulator is ≲2 μm in absence of active stabilization. However, evaporation in the hybrid trap is adaptable to a wide range of z_0 except for a z_0 so large that it is difficult to make the adiabatic transport from the magnetic to the dipole trap and that it weakens the harmonic confinement along $\hat{y}$.

During the 3 s loading to the dipole trap, the truncation parameter η increases from 6 to 10 due to the rf knife and ≈0.2 s of free evaporation at the end. The atom number decreases by a factor of ≈4, arising from both the rf evaporation and the loss of atoms in the low-density tails at $B'\sim mg/\mu$. Figure 8 shows the temperature T versus the quadrupole field gradient B' during the loading. The entropy per atom S/Nk_B is initially 31.5, then it slightly decreases by ≲1.5, and the cloud cools from $T=30$ to 5.2 μK.

After loading the atoms into the dipole trap, we then perform forced evaporation by lowering the dipole trap depth from 49(6) μK to a variable U in 4 s and simultaneously decrease B' from 0.30 to 0.27 T m^{-1}. The trap depth versus time is approximately quadratic, slower toward the end the evaporation. At $U=4.7(7)$ μK, a bimodal distribution in the

time-of-flight (TOF) image shows a 6% condensation fraction of the total number $N=4\times10^6$ with a temperature $T=0.32(5)$ μK (calculated $T_c=0.5$ μK). At $U=1.4(2)$ μK, the condensate is nearly pure with $N=1.8\times10^6$. Figure 9 shows the atom number N and the temperature T versus the trapping time and the evolution of phase-space density D versus N in the following steps: (i) rf evaporation in the magnetic trap, (ii) transfer to the dipole trap, and (iii) evaporation in the dipole trap.

We have also successfully produced condensates with similar atom numbers adopting the same hybrid technique using different dipole beam parameters. They include: (1) a different waist $w_0\sim90$ μm still at $\lambda=1550$ nm and (2) a different wavelength $\lambda=1064$ nm and waist $w_0\sim70$ μm. The robustness of our approach to these changes illustrates the generality and versatility of such hybrid magnetic and optical trapping approach.

IV. CONCLUSION

We have described a simple and effective technique of producing ^{87}Rb Bose-Einstein condensates which merges the best aspects of magnetic and optical trapping. A condensate of $\sim2\times10^6$ atoms is produced in a cycle time of 16 s. This approach applies for a wide range of trap parameters, such as the quadrupole field gradient, the dipole beam trap depth, and the waist. We expect that this technique can be generally applicable to other magnetically trappable atomic species.

ACKNOWLEDGMENTS

This work was partially supported by ONR, ODNI, ARO with funds from the DARPA OLE program, and the NSF through the JQI Physics Frontier Center. R.L.C. acknowledges supports from NIST/NRC.

[1] Bose condensation of atomic hydrogen is an exception where the initial cold atomic sample was prepared not by laser cooling but instead by thermalization with a buffer gas [26].
[2] M. H. Anderson, J. R. Ensher, M. R. Matthews, C. E. Wieman, and E. A. Cornell, Science **269**, 198 (1995).
[3] K. B. Davis, M. O. Mewes, M. R. Andrews, N. J. van Druten, D. S. Durfee, D. M. Kurn, and W. Ketterle, Phys. Rev. Lett. **75**, 3969 (1995).
[4] A. L. Migdall, J. V. Prodan, W. D. Phillips, T. H. Bergeman, and H. J. Metcalf, Phys. Rev. Lett. **54**, 2596 (1985).
[5] K. B. Davis, M.-O. Mewes, M. A. Joffe, M. R. Andrews, and W. Ketterle, Phys. Rev. Lett. **74**, 5202 (1995).
[6] W. Petrich, M. H. Anderson, J. R. Ensher, and E. A. Cornell, Phys. Rev. Lett. **74**, 3352 (1995).
[7] D. S. Naik and C. Raman, Phys. Rev. A **71**, 033617 (2005); I. Bloch (private communication); M. Raizen (private communication).
[8] M. D. Barrett, J. A. Sauer, and M. S. Chapman, Phys. Rev. Lett. **87**, 010404 (2001).
[9] T. Weber, J. Herbig, M. Mark, H. C. Nagerl, and R. Grimm, Science **299**, 232 (2003).
[10] G. Cennini, G. Ritt, C. Geckeler, and M. Weitz, Appl. Phys. B **77**, 773 (2003).
[11] T. Kinoshita, T. Wenger, and D. S. Weiss, Phys. Rev. A **71**, 011602(R) (2005).
[12] D. Comparat, A. Fioretti, G. Stern, E. Dimova, B. Laburthe Tolra, and P. Pillet, Phys. Rev. A **73**, 043410 (2006).
[13] O. J. Luiten, M. W. Reynolds, and J. T. M. Walraven, Phys. Rev. A **53**, 381 (1996).
[14] W. Ketterle and N. J. vanDruten, Adv. At., Mol., Opt. Phys. **37**, 181 (1996).
[15] D. M. Stamper-Kurn, H. J. Miesner, A. P. Chikkatur, S. Inouye, J. Stenger, and W. Ketterle, Phys. Rev. Lett. **81**, 2194 (1998).
[16] J. F. O'Hanlon, *A User's Guide to Vacuum Technology*, 3rd ed. (Wiley, New York, 2003).
[17] L. V. Hau, J. A. Golovchenko, and M. M. Burns, Rev. Sci. Instrum. **65**, 3746 (1994).
[18] M. R. Walkiewicz, P. J. Fox, and R. E. Scholten, Rev. Sci. Instrum. **71**, 3342 (2000).
[19] A. Pailloux, T. Alpettaz, and E. Lizon, Rev. Sci. Instrum. **78**, 023102 (2007).
[20] H. C. W. Beijerinck and N. F. Verster, J. Appl. Phys. **46**, 2083 (1975).
[21] S. L. Rolston (private communication).
[22] W. D. Phillips and H. Metcalf, Phys. Rev. Lett. **48**, 596 (1982).
[23] A. Witte, T. Kisters, F. Riehle, and J. Helmcke, J. Opt. Soc. Am. B **9**, 1030 (1992).
[24] C. J. Dedman, J. Nes, T. M. Hanna, R. G. Dall, K. G. H. Baldwin, and A. G. Truscott, Rev. Sci. Instrum. **75**, 5136 (2004).
[25] Uncertainties reflect the uncorrelated combination of $1-\sigma$ statistical and systematic uncertainties.
[26] D. G. Fried, T. C. Killian, L. Willmann, D. Landhuis, S. C. Moss, D. Kleppner, and T. J. Greytak, Phys. Rev. Lett. **81**, 3811 (1998).